Chinese Chemical Letters 32 (2021) 375–379

Contents lists available at ScienceDirect

Chinese Chemical Letters

journal homepage: www.elsevier.com/locate/cclet

Communication

Cucurbit[*n*]uril-calix[*n*]arene-based supramolecular frameworks assembled using the outer surface interactions of cucurbit[*n*]urils

Ming Liu[a], Yang Zhou[b], Lixia Chen[a], Bing Bian[c], Xin Xiao[a,*], Zhu Tao[a,*]

[a] Key Laboratory of Macrocyclic and Supramolecular Chemistry of Guizhou Province, Guizhou University, Guiyang 550025, China
[b] College of Chemistry, Chemical Engineering and Materials Science, Shandong Normal University, Ji'nan 250014, China
[c] College of Chemical and Environmental Engineering, Shandong University of Science and Technology, Qingdao 266590, China

ARTICLE INFO

Article history:
Received 23 December 2019
Received in revised form 27 February 2020
Accepted 15 March 2020
Available online 18 March 2020

Keywords:
Cucurbit[*n*]urils
Calix[*n*]arene
Outer surface interaction of Q[*n*]s
Supramolecular frameworks
Functional properties

ABSTRACT

Based on the crystal structures of two cucurbit[6]uril/calix[*n*]arene-based supramolecular frameworks reported by Long and co-workers, we further investigated the interactions of cucurbit[6]uril with 4-sulfocalix[4]arene and 4-sulfocalix[6]arene using ^{1}H NMR spectroscopy and isothermal titration calorimetry (ITC), respectively. Moreover, solid fluorescent materials were prepared *via* the adsorption of fluorescent dyes by these porous supramolecular frameworks, which exhibit a selective response to certain volatile organic compounds.

Recent research has shown that Q[*n*]-based frameworks are very common in Q[*n*] chemistry, involving Q[*n*]-based coordination chemistry [1–7], Q[*n*]-based host-guest chemistry [8–10] and, in particular, Q[*n*]-based outer surface interaction chemistry [11,12] due to the surface electrostatic potential of Q[*n*]s, namely their two electrically negative opening portals (red in Fig. 1), their almost electrically neutral inner cavity surface (yellow in Fig. 1) and their electrically positive outer surface (blue in Fig. 1). Herein, we focus on the recent progress toward the design and construction of Q[*n*]-based supramolecular frameworks (QSFs) assembled using the outer surface interactions of Q[*n*]s (OSIQ). QSFs through the OSIQ can be classified as those assembled by i) a self-structure-directing effect; ii) the interaction of inorganic anions with the outer surfaces of Q[*n*]s and iii) the interaction of aromatic compounds with the outer surfaces of Q[*n*]s. Fig. 2 shows a schematic representation of these three typical OSIQs. The first case is the simplest, namely the dipole interaction between the portal carbonyl oxygen atoms in the Q[*n*] molecule and the outer surface of the adjacent Q[*n*] molecules, including the portal carbonyl carbon atoms, bridged methylene units and methine units in the glycouril moieties of the adjacent Q[*n*] molecules. The second case involves with the ion-dipole interaction between various inorganic anions and the outer wall of the adjacent Q[*n*] molecules, including the portal carbonyl carbon atoms, bridged methylene units and methine units in the glycouril moieties of the adjacent Q[*n*] molecules, while the inorganic anions include inorganic acid anions, transition metal polychlorinated anions, especially polyacid and heteropolyacid anions. The third case involves with $\pi\cdots$interactions formed between carbonyl group on the outer surface of the Q[*n*] molecule and aromatic compounds, C-H$\cdots\pi$ interactions between the methylene and methine groups on the outer surface of the Q[*n*] molecule and aromatic compounds, and so on.

One of the aromatic compounds studied is the calix[*n*]arenes (C[*n*]As), which are characterized by not only a hydrophobic cavity, but also n phenyl rings bridged by n methylene groups. Therefore, C[*n*]As are not only a kind of macrocyclic compound that can also be used construct various C[*n*]A-based sensors and supramolecular frameworks [13–15], but also play a role of the structure directing agent, resulting in the formation of novel Q[*n*]/C[*n*]A-based supramolecular frameworks [16,17]. Moreover, in order to increase their water solubility, hydrophilic groups such as sulfonated groups are often introduced into C[*n*]As to form 4-sulfocalix[*n*]arenes (SC[*n*]As) and so on, which have not only an aromatic ring, but also an anion. SC[*n*]As exhibit stronger interactions with Q[*n*]s *via* OSIQ and can construct various Q[*n*]/C[*n*]A-based supramolecular frameworks. As early as 2008, Long and co-workers chose 4-sulfocalix[*n*]arenes (SC[*n*]As; $n = 4$ and 6) and Q[6] as building blocks. By using the OSIQ, they first obtained precipitates from the Q[6]-SC[4] and Q[6]-SC[6] reaction systems

* Corresponding authors.
E-mail addresses: gyhxxiaoxin@163.com (X. Xiao), gzutao@263.net (Z. Tao).

https://doi.org/10.1016/j.cclet.2020.03.042
1001-8417/

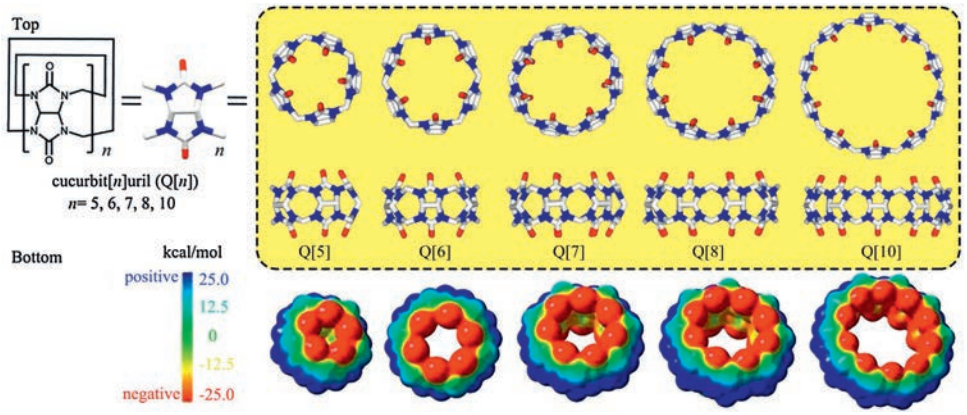

Fig. 1. (Top) X-ray crystal structures of five common Q[*n*]s, namely Q[5], Q[6], Q[7], Q [8] and Q[10]. (Bottom) Electrostatic potential maps (ESPs) obtained for Q[5], Q[6], Q[7], Q[8] and Q[10].

from an aqueous solution of HCl (3.0 mol/L). They then dissolved the precipitate obtained from the Q[6]-SC[4] reaction system in an aqueous solution of HCl (6.0 mol/L) and the precipitate obtained from the Q[6]-SC[4] reaction system by adjusting the pH to 7 using 1.0 mol/L ammonia solution, respectively. The solutions were allowed to stand in the air until crystals occurred. Long and co-workers characterized the structures of these two crystals using single crystal X-ray diffraction and described their novel frameworks in detail (Figs. S1 and S2 in Supporting information) [16]. Herein, we only emphasize that the OSIQ plays an important role in constructing the Q[6]/SC[4]A- and Q[6]/SC[6]A-based supramolecular frameworks (**1** and **2**). Fig. 3a shows the relationship between each Q[6] molecule in **1** (in yellow) and the adjacent Q[6] and SC[4]A molecules, including the dipole interactions with the portal carbonyl oxygen atoms in two adjacent Q[6] molecules with the methine units on the outer surface of the central Q[6] molecule (Fig. 3b), the dipole interactions with the oxygen atoms of the sulfonated groups in the SC[4]A molecules with the bridged methylene units on the outer surface of the central Q[6] molecule (Fig. 3c) and the π···interactions between the carbonyl group on the outer surface of the central Q[6] molecule and aromatic ring on SC[4]A molecules, C-H···π interaction between methylene and methine groups on the outer surface of the central Q[6] molecule and aromatic ring in the SC[4]A molecules (Fig. 3d).

Unlike **1**, the Q[6] molecules are isolated by the SC[6]A molecules in **2**. There are two different relationships between the Q[6] molecule and SC[6]A molecules: A Q[6] molecule (in yellow) is surrounded by four SC[6]A molecules (Fig. 3e) and Fig. 3f shows the detailed interaction of the central Q[6] molecule with the adjacent SC[6]A molecule through the OSIQ, including the π···interaction between the carbonyl group on the outer surface of the central Q[6] molecule and the aromatic rings in the SC[6]A molecules (in red dashed line), C-H···π interactions between the methylene and methine groups on the outer surface of the central Q[6] molecule and the aromatic rings in the SC[6]A molecules (in blue dashed line) and the dipole interaction between the oxygen atoms of the sulfonated groups in the SC[6]A molecules and the bridged methylene and methine units on the outer surface of the central Q[6] molecule (in black dashed line). The Q[6] molecule (in green) is supported by two SC[6]A molecules, Figs. 3g and h show the detailed interactions between the Q[6] molecule (in green) with the adjacent SC[6]A molecules through the OSIQ, which is similar to those in the above case.

Powder X-ray diffraction analysis of **1** and **2** accompanied by simulations revealed that the bulk of the samples essentially consisted of pure crystalline phases (Figs. S3 and S4 in Supporting information). Analysis of the thermal stabilities of **1** and **2** by thermogravimetry is deposited in Supporting information (Figs. S5 and S6 in Supporting information).

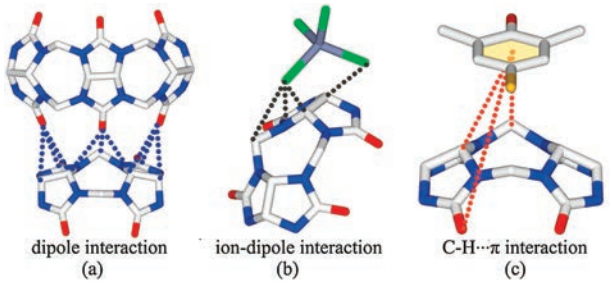

Fig. 2. A schematic representation of the outer surface interactions formed between the Q[*n*] molecule and different compounds.

We further investigated the interactions between Q[6] and SC[*n*]As (n = 4 or 6) in solution using isothermal titration calorimetry (ITC) and ^{1}H nuclear magnetic resonance (^{1}H NMR) spectroscopy. ITC experiments were carried out to quantify the association constants and thermodynamic parameters of the interactions between Q[6] and SC[*n*]As (n = 4 or 6), respectively in an aqueous solution (Fig. 4). The data obtained from the ITC experiments (Table 1) revealed that the interactions between Q[6] and SC[*n*]As (n = 4 or 6) are exclusively enthalpydriven. The high enthalpy value may be a result from the stronger OSIQ between the Q[6] molecules and SC[*n*]A (n = 4 or 6) molecules. Meanwhile, their free movement was also limited (Entropy reduction processes). The moderate association constants obtained for Q[6]/SC[4]A and Q[6]/SC[6]A were [Ka = $(1.03 \pm 0.04) \times 10^4$ L/mol] and Ka = $(3.61 \pm 0.07) \times 10^4$ L/mol, respectively.

In order to confirm the composition of the precipitate obtained from the Q[6]-SC[4]A and Q[6]-SC[6]A interaction systems, ^{1}H NMR spectroscopy was carried out by dissolving the precipitate in a DCl/D_2O solution (4 mol/L) and comparing the spectrum with that recorded for free Q[6], SC[4]A and SC[6]A, respectively. Figs. 5a-c show the ^{1}H NMR spectra recorded for free Q[6], free SC [4]A and the precipitate obtained from the Q[6]-SC[4]A interaction system. By comparing free SC[4]A with the SC[4]A in the precipitate, we found that the proton resonances of the SC[4]A molecule in the precipitate are shifted downfield by 0.04 and 0.05 ppm, respectively. However, the proton resonances of Q[6] before and after interacting with SC[4]A remain unchanged. Moreover, the integral intensity of Q[6] and SC[6]A in Fig. 5e indicates that the interaction ratio of the two building blocks was 1:1. Figs. 5a, d and e show the ^{1}H NMR spectra recorded for free Q [6], free SC[6]A, and the precipitate obtained from the Q[6]-SC[6]A

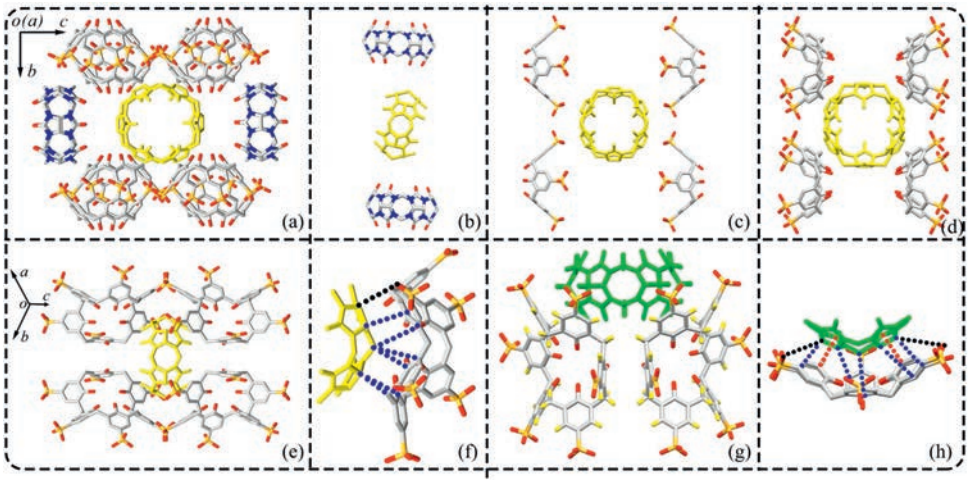

Fig. 3. Crystal structure of **1**: (a) Overall OSIQ of a Q[6] molecule (in yellow) with the adjacent Q[6] and SC[4]A molecules including (b) two adjacent Q[6] molecules, (c) four SC[4]A molecules and (d) four SC[4]A molecules. Crystal structure of **2**: (e) The relationship between the Q[6] molecule (in yellow) with four adjacent SC[6]A molecules, (f) detailed OSIQ between the yellow Q[6] molecule and the adjacent SC[6]A molecules, (g) the relationship between the Q[6] molecule (in green) with two adjacent SC[6]A molecules and (h) detailed OSIQ between the green Q[6] molecule and the adjacent SC[6]A molecules.

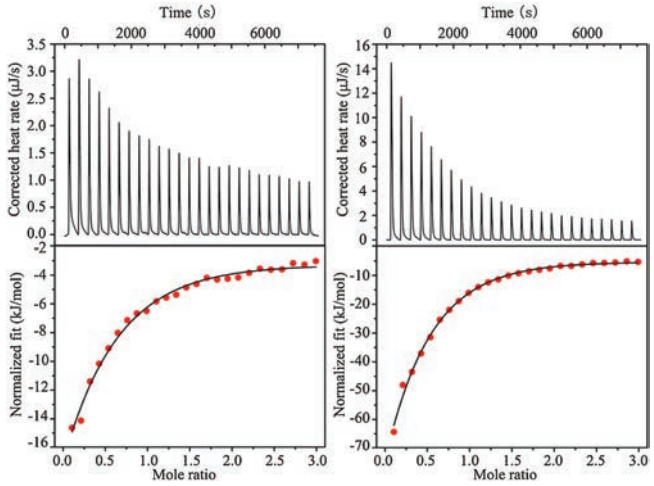

Fig. 4. Isothermal titration calorimetry profiles obtained for Q[6] in the presence of SC[4]A (left) and SC[6]A (right) in an aqueous solution at 298.15 K.

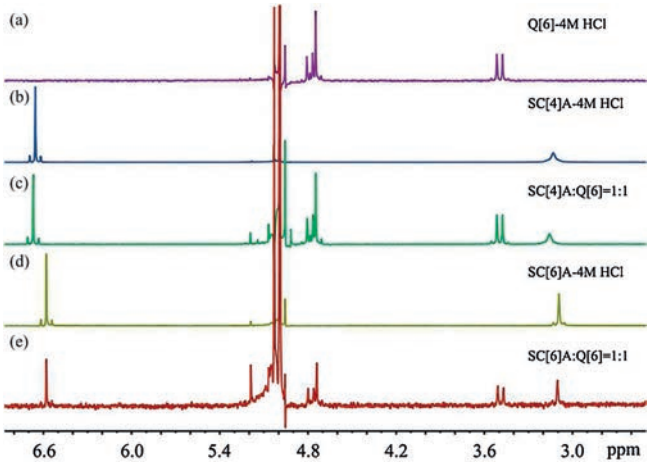

Fig. 5. ^{1}H NMR spectra of (a) free Q[6], (b) free SC[4]A, (c) the precipitate obtained from the Q[6]-SC[4]A interaction system in 4 mol/L DCl/D_2O, (d) free SC[6]A and (e) the precipitate obtained from the Q[6]-SC[6]A interaction system in 4 mol/L DCl/D_2O.

Table 1
Thermodynamic parameters obtained for Q[6] with SC[*n*]As (*n* = 4 or 6) in an aqueous solution at 298.15 K.

Q[6]/SC[*n*]As	*Ka* (L/mol)	Δ*H* (kJ/mol)	*T*Δ*S* (kJ/mol)
Q[6]/SC[4]A	$(1.03 \pm 0.04) \times 10^4$	−99.6	−76.7
Q[6]/SC[6]A	$(3.61 \pm 0.07) \times 10^4$	−100.0	−74.0

interaction system. Unlike the Q[6]-SC[4]A interaction system, both proton resonances observed for Q[6] and SC[6]A in the precipitate remain unchanged when compared with free Q[6] and SC[6]A.

Based on the crystal structures of the Q[6]/SC[4]A- and Q[6]/SC[6]A-based supramolecular frameworks (**1** and **2**), we understand that there are a large number of pores and channels in these solid compounds. Whether these pores and channels can be used for selective adsorption of fluorophore dyes (FDs) to form fluorescent materials is a research subject that we pay special attention to. Many of our previous studies have proven that Q[*n*]-based supramolecular frameworks exhibit adsorption capacities for various FDs to become novel luminescent materials [18–20]. However, the use of Q[*n*]/C[*n*]A-based supramolecular frameworks to prepare fluorescent materials is rare [17]. A general survey of loading **1** and **2** with over 40 selected FDs, respectively (Table S1 in Supporting information) to form luminescent FD@**1** and FD@**2** was carried out and several samples exhibited a significant fluorescence enhancement. For example, loading **1** with levofloxacin (FD4) formed luminescent FD4@**1** with a significant fluorescence enhancement (Fig. 6a), loading **2** with naphthol (FD29) formed luminescent FD29@**2** with a fluorescence enhancement (Fig. 6b) and the fluorescence intensity increased 1.34- and 0.76-fold, respectively when compared with the results of the adsorption of their corresponding FDs. On the other hand, after the adsorption of FD4 by free Q[6] and free SC[4]A, and FD29 by free Q[6] and free SC[6]A, the fluorescence intensities of the FD4@Q[6], FD4@SC[4]A, FD29@Q[6] and FD29@SC[6]A products were either unchanged or lower (Fig. 6).

Moreover, the FD@Q[6]/SC[*n*]As do not only become fluorescence materials, but also sensors for some volatile organic compounds. The detailed description of the adsorption and

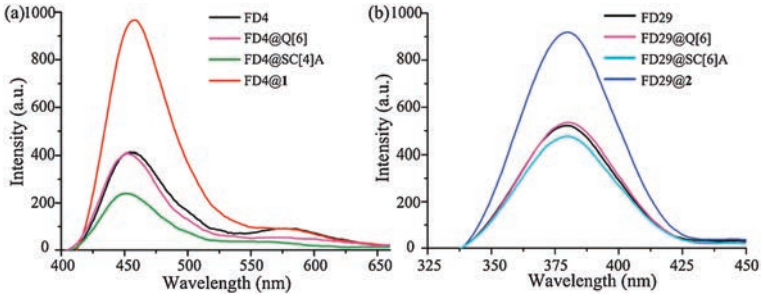

Fig. 6. The fluorescence spectra recorded for (a) free FD4, FD4@Q[6], FD4@SC[4]A and FD4@**1**, and (b) free FD29, FD29@Q[6], FD29@SC[6]A and FD29@**2**.

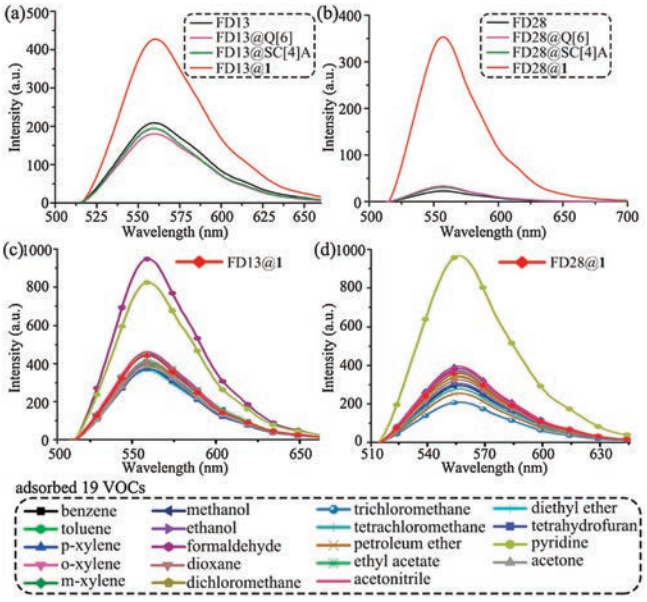

Fig. 7. The fluorescence spectra recorded for (a) free FD13, FD13@Q[6], FD13@SC[4]A and FD13@**1**, and (b) free FD28, FD28@Q[6], FD28@SC[4]A and FD28@**1**. The general survey fluorescence spectra recorded for (c) FD13@**1** and (d) FD28@**1** loaded with 19 VOCs, respectively.

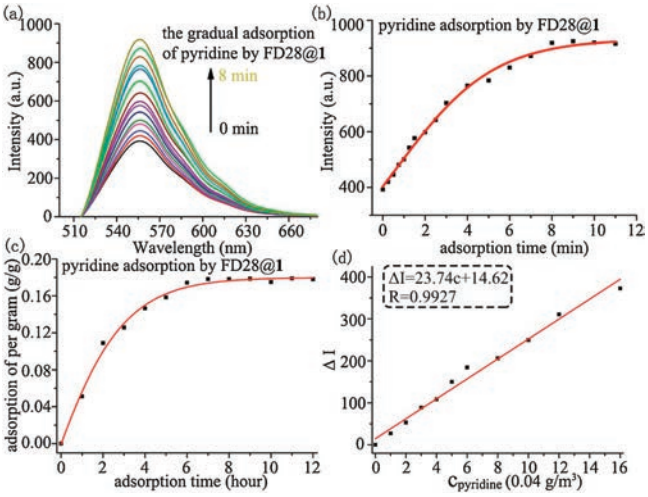

Fig. 8. Time-resolved fluorescence spectra recorded for the loading of (a) FD28@**1** with pyridine and the changes in the fluorescence intensity of (b) FD28@**1** loaded pyridine upon increasing the adsorption time. The adsorption profiles obtained for the loading of (c) pyridine on FD28@**1** and (d) plots of ΔI *vs.* the amount of pyridine on FD28@**1**.

desorption analysis of the responses of FDs@**1** to volatile organic compounds is shown in Supporting information. For example, loading **1** with astrazon pink FG (FD13) can form luminescent FD13@**1** with double fluorescence enhancement (Fig. 7a), which exhibits a highly selective response to formaldehyde and pyridine in 19 common volatile organic compounds (VOCs) via further fluorescence enhancement (Fig. 7c). Moreover, loading **1** with methyl red (FD28) can form luminescent FD28@**1** with a 14-fold fluorescence enhancement (Fig. 7b), which exhibited a highly selective response to pyridine in 19 common VOCs via further fluorescence enhancement (Fig. 7d). From the detailed time-resolved adsorption fluorescence spectra recorded for solid FD28@**1** during the gradual adsorption of pyridine gas, (Fig. 8a), the plots of the fluorescence intensities (I_f) of solid FD28@**1** *vs.* the adsorption time of pyridine gas and solid FD28@**1** *vs.* the adsorption time of pyridine gas, respectively were drawn in Fig. 8b and the plots of the amount of formaldehyde and pyridine adsorbed on solid FD28@**1** *vs.* time, respectively (Fig. 8c). Based on the data obtained for I_f *vs.* time (Fig. 8b) and the amount of adsorbed VOCs *vs.* time (Fig. 8c), the plots of ΔI *vs.* the amount of adsorbed VOCs on solid FD28@**1** were constructed (Fig. 8d). Thus, the detection limits (DL) of FD28@**1** and FD28@**1** for pyridine were then calculated by multiplying the standard deviation of ten measurements in the absence of metal cations by three and then dividing by the slope of the linear calibration plot over a low concentration range. The DL of solid FD28@**1** for pyridine was determined to be 0.25 mg/m^3, respectively.

Some control experiments for the adsorption of formaldehyde and pyridine for FD13@Q[6], FD13@SC[4]A, FD28@Q[6] and FD28@SC[4]A, respectively, has also been carried out (Figs. S9-S11 in Supporting information), which exhibited almost no change in fluorescence emission intensity before and after the amorphous solid FD13@Q[6], FD13@SC[4]A, FD28@Q[6] or FD28@SC[4]A adsorbed formaldehyde and pyridine. This was in stark contrast to the strong fluorescence emission enhancement seen for after supramolecular assembly FD13@**1**, FD28@**1** adsorbed formaldehyde and pyridine, suggesting that amorphous Q[6] and SC[4]A powder do not provide suitable channels to accommodate FD13, FD28, formaldehyde and pyridine, that is, cannot restrains the free movement of the two fluorophore dyes and specific VOCs. The details of the reversibility of formaldehyde and pyridine adsorption experiments are deposited in Supporting information (Figs. S12-S14 in Supporting information). The formaldehyde and pyridine recognition process of the FD13@**1** and FD28@**1** supramolecular assembly is thus irreversible, therefore, the potential application of FD13@**1** and FD28@**1** for the recognition of formaldehyde and pyridine would be restricted to a one-time detection. Loading the FD13@**1** supramolecular assembly with acetaldehyde also resulted in dramatic fluorescence enhancement of the FD13@**1** system, this result further supported the conclusion

of reaction of FD13 with aldehydes (Fig. S15 in Supporting information).

In this work, we repeated the work reported by Long *et al.* [16], in which two Q[*n*]/SC[*n*]A-based supramolecular frameworks (**1** and **2**) were constructed from Q[6] and SC[*n*]As (*n* = 4 or 6), respectively. The interaction ratio of Q[6]:SC[*n*]As (*n* = 4 or 6) in **1** and **2** was 1:1 and the OSIQ was the driving force resulting in the formation of the Q[*n*]/SC[*n*]A-based supramolecular frameworks. ITC experimental results revealed that the interaction of Q[6] with SC[*n*]As (*n* = 4 or 6) were enthalpy-driven because the strong OSIQ formed between Q[6] with SC[*n*]As (*n* = 4 or 6) restrains the free movement of the two species. The adsorption experiment have further proven that Q[6]/SC[*n*]A-based (*n* = 4 or 6) supramolecular frameworks can adsorb various fluorophore dyes (FDs) to form solid fluorescence materials (FD@Q[6]/SC[*n*]As). Moreover, these materials can become highly selective sensors for certain volatile organic compounds. After understanding the characteristics of the Q[*n*]/C[*n*]A-based supramolecular frameworks and confirming their adsorption capacity, we will focus on the fluorescence enhancement mechanism of FD loaded on Q[*n*]/C[*n*]A-based supramolecular frameworks and the identification principle of specific VOCs using these frameworks in future studies.

Declaration of competing interest

The authors declare no competing financial interest.

Acknowledgments

We acknowledge the financial support of National Natural Science Foundation of China (Nos. 51663005, 21761007 and 21871064), Science and Technology Plan Project of Guizhou Province (Nos. 20175788 and 20185781), the Creative Research Groups of Guizhou Provincial Education Department (No. 2017-028), the Innovation Program for High-level Talents of Guizhou Province (No. 20165657) and "Chun-Hui" Fund of Chinese Ministry of Education (No. Z2017005).

Appendix A. Supplementary data

Supplementary material related to this article can be found, in the online version, at doi:https://doi.org/10.1016/j.cclet.2020.03.042.

References

[1] X.L. Ni, J.X. Lin, Y.Y. Zheng, et al., Cryst. Growth Des. 8 (2008) 3446–3450.
[2] P. Thuery, Cryst. Growth Des. 8 (2008) 4132–4143.
[3] P. Thuery, CrystEngComm. 11 (2009) 1150–1156.
[4] Z.F. Li, F. Wu, F.G. Zhou, et al., Cryst. Growth Des. 10 (2010) 5113–5116.
[5] Z.F. Li, L.L. Liang, F. Wu, et al., CrystEngComm 15 (2013) 1994–2001.
[6] H. Cong, Y. Zhao, L.L. Liang, et al., Eur. J. Inorg. Chem. (2014) 2262–2267.
[7] N.N. Ji, X.J. Cheng, L.L. Liang, et al., CrystEngComm 15 (2013) 7709–7717.
[8] J. Tian, H. Wang, D.W. Zhang, Y. Liu, Z.T. Li, Natl. Sci. Rev. 4 (2017) 426–436.
[9] J. Tian, L. Chen, D.W. Zhang, Y. Liu, Z.T. Li, Chem. Commun. 52 (2016) 6351–6362.
[10] J. Tian, Z.Y. Xu, D.W. Zhang, et al., Nat. Commun. (2016) 11580.
[11] D. Bardelang, K.A. Udachin, D.M. Leek, et al., Cryst. Growth Des. 11 (2011) 5598–5614.
[12] X.L. Ni, X. Xiao, H. Cong, et al., Acc. Chem. Res. 47 (2014) 1386–1395.
[13] X.Y. Lou, Y.P. Li, Y.W. Yang, Biotechnol. J. 14 (2019) 1800354.
[14] H. Zhang, R. Zou, Y. Zhao, Coord. Chem. Rev. 292 (2015) 74–90.
[15] Olivia Bistri, Olivia Reinaud, Org. Biomol. Chem. 13 (2015) 2849–2865.
[16] R.G. Lin, L.S. Long, R.B. Huang, L.S. Zheng, Cryst. Growth Des. 8 (2008) 791–794.
[17] X. Tian, L.X. Chen, Y.Q. Yao, et al., ACS Omega 3 (2018) 6665–6672.
[18] Y.Q. Yao, Y.J. Zhang, Y.Q. Zhang, et al., ACS Appl. Mater. Inter. 9 (2017) 40760–40765.
[19] M. Liu, J.L. Kan, Y.Q. Yao, et al., Sensor. Actuat. B: Chem. 283 (2019) 290–297.
[20] M. Liu, M.X. Yang, Y.Q. Yao, et al., J. Mater. Chem. C 7 (2019) 1597–1603.